Chem Soc Rev

To rebound or dissociate? This is the mechanistic question in C-H hydroxylation by heme and nonheme metal-oxo complexes

Journal:	*Chemical Society Reviews*
Manuscript ID	CS-SYN-07-2015-000566.R2
Article Type:	Tutorial Review
Date Submitted by the Author:	24-Oct-2015
Complete List of Authors:	Cho, Kyung-Bin; Ewha Womans University, Chemistry and Nano Science Hirao, Hajime; Nanyang Technological University, Shaik, Sason; The Hebrew University, Institute of Chemistry Nam, Wonwoo; Ewha Womans University, Chemistry

Journal Name

ARTICLE

To rebound or dissociate? This is the mechanistic question in C-H hydroxylation by heme and nonheme metal-oxo complexes

Kyung-Bin Cho,*[a] Hajime Hirao,*[b] Sason Shaik*[c] and Wonwoo Nam*[a]

Received 00th January 20xx,
Accepted 00th January 20xx

DOI: 10.1039/x0xx00000x

www.rsc.org/

Enzymatic reactions that involve C-H bond activation of alkanes by high-valent iron-oxo species can be explained by the so-called rebound mechanism (RM). Hydroxylation reactions of alkane substrates effected by the reactive Compound I (Cpd I) species of cytochrome P450 enzymes are good examples. There was initially little doubt that the rebound paradigm could be carried over in the same form to the arena of synthetic nonheme high-valent iron-oxo or other metal-oxo complexes. However, the active reaction centers of these synthetic systems are not well-caged, in contrast to the active sites of enzymes; therefore, the relative importance of the radical dissociation pathway can become prominent. Indeed, accumulating experimental and theoretical evidence shows that introduction of the non-rebound mechanism (non-RM) is necessary to rationalise the different reactivity patterns observed for synthetic nonheme complexes. In this tutorial review, we discuss several specific examples invloving the non-RM while making frequent comparisons to the RM, mainly from the perspective of computational chemistry. We also provide a technical guide to DFT calculations of RM and non-RM and to the interpretations of computational outcomes.

1. Introduction

Heme and nonheme enzymes that monooxygenate a variety of organic compounds with high efficiency and specificity have attracted much interest in the biological and chemical communities for more than four decades. One of the unique features of these enzymes is their ability to hydroxylate C-H bonds with high stereo- and regioselectivites. A few examples are shown in Scheme 1. The heme enzyme Cytochrome $P450_{cam}$ hydroxylates camphor specifically at the 5-exo position, while $P450_{BM3}$ hydroxylates fatty acids at the ω-1/ω-2 positions but not in the endmost ω position. Similarly, the nonheme enzyme taurine:αKG dioxygenase (TauD) hydroxylates taurine (2-aminoethanesulfonic acid) at the α-CH_2 position adjacent to the sulfate substituent.

The mechanism that appears to unify all these and other data is called the "rebound mechanism" (RM),[1] and its key features are described in Learning Box 1 and Scheme 2a. Inspection of the singly occupied π* and/or σ* type orbitals (*vide infra*) shows clearly that the ferryl moiety has an oxyl radical with spin density of 1.0 or so. Accordingly, the RM in Scheme 2a starts with hydrogen atom (H-atom) abstraction that leads to the $Fe^{IV}OH$/Alk• species in the cage, in which an alkyl radical, Alk•, interacts weakly with the $Fe^{IV}OH$ species. This process is followed by a rebound of the carbon radical to the OH moiety of the $Fe^{IV}OH$ species, resulting in formation of an alcohol product, Alk-OH. The rate-determining step is the H-atom abstraction, and therefore a kinetic isotope effect (KIE) arises when D replaces H. The rebound step is very fast, having an energy barrier ranging from zero to a few kcal mol^{-1}.[2] Therefore, if the radical is well-caged, the Alk-OH product will be formed with a high degree of retention of stereochemistry. If, however, the cage allows escape, the radical dissociates, leaves the cage, and undergoes rearrangement,[3,4] and then the rebound takes place. Similarly, if the radical-rearrangement barrier is smaller than the rebound barrier, the reaction may involve an in-cage rearrangement before the rebound takes place, thus yielding a rearranged Alk-OH product.

Formulation of the RM was an epoch-making event in the mechanistic study of metal-oxo complexes, because it unified much of the known data and articulated how experiments should be designed to trap radicals and determine their lifetimes.[1,5–7] As in the case of any evolution of knowledge, it is instructive to look at the mechanistic understanding of the pre-rebound era[8] and appreciate how desperately such a unified mechanism was needed to establish an overarching paradigm for research. There have been quite a few contributors to this

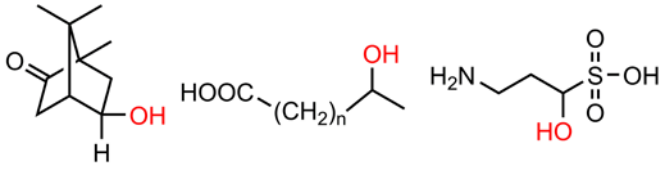

Scheme 1. Hydroxylation products of camphor, a fatty acid, and taurine.

[a] Department of Chemistry and Nano Science, Ewha Womans University, Seoul 03760, Korea. Email: workforkyung@ewha.ac.kr, wwnam@ewha.ac.kr
[b] Division of Chemistry and Biological Chemistry, School of Physical and Mathematical Sciences, Nanyang Technological University, 21 Nanyang Link, Singapore 637371, Republic of Singapore. Email: hirao@ntu.edu.sg
[c] Institute of Chemistry and The Lise Meitner-Minerva Center for Computational Quantum Chemistry, The Hebrew University of Jerusalem, 91904 Jerusalem, Israel. Email: sason@yfaat.ch.huji.ac.il

† Electronic Supplementary Information (ESI) available: Figures S1-S3. See DOI: 10.1039/x0xx00000x

mechanism,[1,5] but there seems to be a consensus that the formulation of the mechanism is traced back to the early-to-mid 1970s when the seminal papers by Groves and co-workers came out. The name "rebound" appeared already in 1976.[9] Initially, Groves formulated the mechanism for synthetic nonheme complexes of uncharacterized structures,[9,10] but soon afterwards he and his co-workers shifted to P450 chemistry,[3,4,11] where they used in tandem enzymes[4] and model systems.[3,4,11] Characterization of the first synthetic model using various spectroscopic techniques[11,12] enabled the group to relate the synthetic complexes to the known active species in heme systems.[13] The obtained electronic structure information was used for predicting the trajectory of H-atom abstraction and discussing the steric demand of the trajectory.[3,11] The Groves group determined KIEs, trapped the radical intermediate, and used other criteria to establish the RM. The RM received a great deal of support from rearrangement and scrambling data and from early measurement of radical lifetimes during reactions.[1,5]

During the years, the RM for P450 hydroxylation has been challenged mostly by Newcomb,[6] whose experimental results raised a contentious issue; the putative radicals sometimes had a lifetime even shorter than that of a transition state. The work by Shaik and his co-workers,[2] starting the late 1990s, has shown by computational methods (see Learning Boxes 2 and 3) that the controversy can be resolved if the so called Compound I (Cpd I) of P450, an $Fe^{IV}O$ species supported by a porphyrin π-cation radical ligand ($Por^{+\bullet}Fe^{IV}O$), has two virtually degenerate spin states S = 1/2 and S = 3/2 (*vide infra*) and both of them participate in the product formation. Up to that point, spin state changes during the reactions of biologically relevant species were experimentally known only in simple gas-phase model ion systems.[14] As was shown by Shaik *et al*., one of the spin states of Cpd I, S = 1/2, has no rebound barrier (Fig. 1) and its reaction proceeds in an effectively concerted manner to yield the Alk-OH product. The other, S = 3/2, has a finite rebound barrier (Fig. 1) and hence may lead to rearranged products if the radical rearrangement barrier is smaller than the rebound barrier. As we shall see later, this difference in the second (rebound) barrier height is also the key to understanding the RM vis-a-vis non-RM.

Another challenge to the P450 RM was mounted by postulating that, in addition to the $Por^{+\bullet}Fe^{IV}O$ species, there are several other oxidants that have marker reactions and also lead to rearrangement.[6] One of these is the ferric-hydroperoxide

Learning Box 1

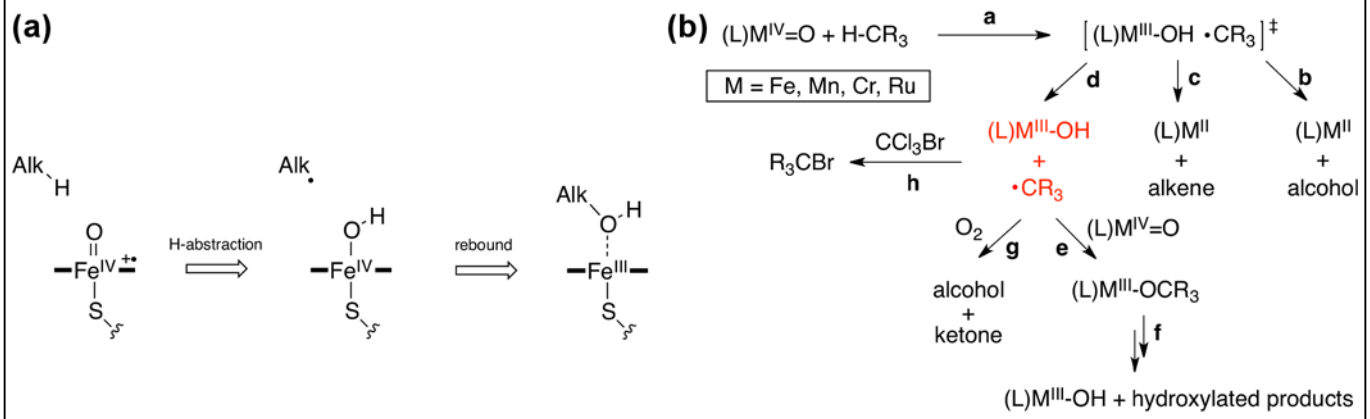

Scheme 2. (a) H-abstraction and rebound steps in P450-catalyzed alkane hydroxylation reactions. (b) Schematic illustration of possible reaction pathways for synthetic nonheme $M^{IV}O$ complexes. The non-RM requires a dissociation of the substrate radical and M^{III}-OH species from the cage (pathway d).

Rebound Mechanism (RM)

The term "oxygen rebound" was first coined by Groves and McClusky to explain the interesting reactivity trend observed when an acetonitrile solution of *m*-chloroperbenzoic acid (*m*-CPBA) was added to cyclohexanol and ferrous perchlorate.[9] It was postulated that an $Fe^{IV}O$ species was generated during the reaction, and interestingly, the oxygen in $Fe^{IV}O$ was exclusively incorporated into the oxygenated product. This result was explained by assuming that the oxygen atom, after abstracting hydrogen, rebounds to the carbon of the substrate (as in the reaction shown in Scheme 2a). The term "oxygen rebound" was also used to describe the behaviour of the oxygen atom in iodosylbenzene (PhIO) in a series of hydroxylation and epoxidation reactions with chloro-α,β,γ,δ-tetraphenylporphinatoiron(III), i.e., a synthetic P450 mimic. Thus, the oxygen first forms a bond with the iron after dissociating from PhIO and subsequently goes to the substrate.[3,12] In practice, rebound usually refers to the radical recombination step in a stepwise reaction of metal-oxo complexes. As discussed in the text, a typical example of RM is the one occurring in the second step of alkane hydroxylation catalyzed by P450 (Scheme 2a), which yields an alcohol product. The RM could affect the reaction outcomes (e.g., selectivity) so critically that having in-depth knowledge of this particular reaction step is certainly beneficial. However, it is not always possible to fully elucidate the reaction mechanisms for metal-oxo species by experiments alone, because the reaction steps involved therein are, more often than not, too fast. This is particularly the case with the rebound step, which is usually not the rate-determining step (Fig. 1). This review explores the possibility of a non-RM pathway, as shown in Scheme 2b, pathway d.

Learning Box 2

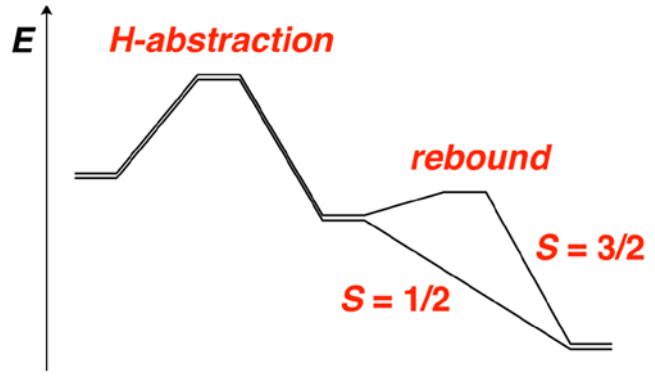

Fig. 1. Typical energy profile for a hydroxylation reaction of Cpd I in P450. The *S* = 1/2 reaction is usually free of a second barrier, while the *S* = 3/2 state does feature a small rebound barrier.

Using Computational Chemistry

Studies using computational chemistry constitute an integral part of the research into the enigmatic reactivity of enzymatic and synthetic metal-oxo complexes. Computational chemistry provides detailed insight into a fast rebound step that features a low or even non-existent energy barrier (Fig. 1). Today, density functional theory (DFT) is the method of choice for studying complex reactive processes of metal-oxo species computationally. Its hybrid version coupled with a molecular mechanics (MM) method (DFT/MM) is also useful in studying reactive metal-oxo species embedded in large enzymes. In most cases, our aim in doing DFT calculations is to optimise structures of intermediates and transition states (TSs) and thereby derive structural and energetic data for the reaction pathway considered. Computational outcomes allow us to delineate an energy landscape for the reaction, and when there is more than one reaction pathway, you can identify the most plausible pathway out of several possible ones, by comparing their computationally estimated stability.

species, PorFe^{III}OOH, which is the precursor of Por$^{+\bullet}$Fe^{IV}O and allegedly prefers C=C double bond epoxidation and heteroatom sulfoxidation. However, as was shown computationally[15] and supported experimentally by using nonheme analogues,[16] this species is a sluggish oxidant in P450 chemistry. A recent work by Rittle and Green[17] has shown that the Por$^{+\bullet}$Fe^{IV}O species is generated in good yield in a working enzyme and is highly reactive to be a competent oxidant. At present, there is no compelling need for additional oxidants in P450 chemistry. All this further buttressed the RM.

In the meantime, the mechanistic study of nonheme iron-oxo systems had been lagging behind. While gas-phase studies of bare metal-oxo ions have been conducted,[18] a model nonheme system was not fully characterized until 2003.[19] In a collaborative work, Nam, Que, and their co-workers succeeded in the synthesis and characterization of a mononuclear nonheme Fe^{IV}O complex, [Fe^{IV}O(TMC)(NCCH$_3$)]$^{2+}$ (TMC = 1,4,8,11-tetramethyl-1,4,8,11-tetraazacyclotetradecane) (Scheme 3). Since then, many new nonheme Fe^{IV}O complexes were synthesized and their H-atom abstraction reactivity was examined. In most of these nonheme cases, the powerful rebound idea served as a paradigm. This idea was boosted by the detection and experimental characterization of the reactive species of some nonheme enzymes, like TauD,[20] which was shown to be the Fe^{IV}O complex in the *S* = 2 state. Since TauD hydroxylates taurine, there was no obvious reason to think that the observed alcohol products in synthetic nonheme chemistry were not the results of the RM. However, there were already tell-tale signs that the hydroxylation mechanism in the *synthetic* nonheme chemistry was different from the known RM in heme systems. For instance, alkane oxidation by various [Fe^{IV}O(TMC)(L$_{ax}$)]$^{z+}$ (L$_{ax}$ = an axial ligand, z = 1 or 2) required two mole equivalents of the Fe^{IV}O oxidant and the iron-complex product was Fe^{III} instead of Fe^{II}.[21] As we shall show below, these and other tell-tale signs indicate that a mechanism different from the RM may well be at work in the chemistry of synthetic nonheme iron-oxo oxidants, in contrast to the cases of heme complexes which still operate via the RM. As the RM has been reviewed many times elsewhere,[5] this tutorial review will focus on the non-RM mainly from a computational chemistry point of view, but with frequent comparisons to the heme-type RM.

2. Possible deviations from rebound mechanism

The RM has been well established and undisputedly shown to occur in many hydroxylation reactions, mostly in heme enzymes. This has led to less scrutiny in new metal-oxo systems, where the RM is seemingly supported at first glance. For instance, the presence of a major hydroxylated product was taken as proof of the rebound process occurring. Some possible indications of contrary (*vide infra*), such as an overall low product yield, could just indicate either low efficiency of the catalyst or difficulty in product analysis. The emergence of Fe^{III} instead of Fe^{II} could also be a result of a secondary reaction (e.g., a comproportionation reaction between Fe^{IV}O and Fe^{II}), and was usually not investigated further. Even theoretical studies have focused in general on describing the RM, although early calculations showed that the dissociation of the radical requires very little energy.[22] Since the first step of the mechanism (i.e., the C-H activation step) is the rate-limiting step, the second step was frequently ignored or found to be so low in barrier that the existence of competitive pathways were considered unlikely.

There were however recurring findings that eventually led to recognition and formulation of an alternative mechanistic

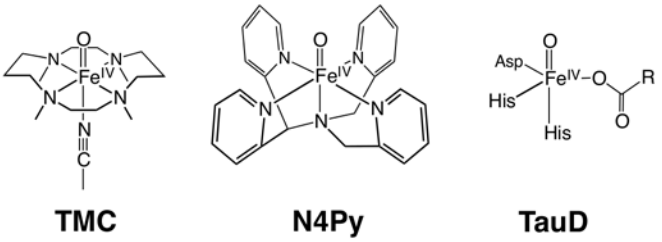

Scheme 3. Examples of two synthetic nonheme Fe^{IV}O complexes, shown along with the TauD-**J** species.

hypothesis to RM (Scheme 2b). Not too long after the first crystal structure of a synthetic nonheme $Fe^{IV}O$ complex was published,[19] C-H activation reactions by two of the earliest synthetic $Fe^{IV}O$ species, $[Fe^{IV}O(N4Py)]^{2+}$ (N4Py = *N*,*N*-bis(2-pyridylmethyl)-*N*-bis(2-pyridyl)methylamine) and $[Fe^{IV}O(Bn\text{-}TPEN)]^{2+}$ (Bn-TPEN = *N*-benzyl-*N*,*N*',*N*'-tris(2-pyridylmethyl)ethane-1,2-diamine), were described in more detail in a thesis work.[23] The fact that the reactions occur through an H-atom abstraction step was verified by establishing a linear correlation between the reaction rates and the C-H bond strengths of a series of substrates, as well as by observing a large KIE upon deuteration. Using triphenylmethane as substrate, the reaction indeed resulted in >95% yield of triphenylmethanol and 80% Fe^{II} products,[23] clearly implying a RM at work. However, using substrates with stronger C-H bonds, the Fe^{II} yield was lowered to ~15%, and the total product yield was gradually reduced as the C-H bonds became stronger. Further, if the reactions were conducted in the presence of air, the yields of the products were higher than 85%. The conclusion was that a minority of the reactions with the stronger C-H bond substrates involve a rebound through the $S = 2$ state (which has a lower rebound barrier), while a majority of the reactions ($S = 1$ state) do not. If air is available, O_2 can interfere with the reaction, showing that the substrate radical does not necessarily have to react with $Fe^{III}OH$ in the second step. These results are, in fact, consistent with non-RM (*vide infra*), which was not formulated at that time.

A second example comes from a recent study on the $[Fe^{IV}O(^{Me,H}Pytacn)(S)]^{2+}$ species (^{Me,H}Pytacn = 1-(2'-pyridylmethyl)-4,7-dimethyl-1,4,7-triazacyclononane, S = CH_3CN or H_2O), which was used to abstract a H-atom from 9,10-dihydroanthracene (DHA).[24] DHA usually does not participate in a rebound reaction because of its weak C-H and C-O bonds, but it is desaturated to form anthracene instead. Indeed, the study identified anthracene as the sole product, with a yield of 45% relative to the $Fe^{IV}O$ catalyst. Since the product solution was dominated by the Fe^{III} species, the authors concluded that DHA was desaturated by two $Fe^{IV}O$ species, forming two $Fe^{III}OH$ species per anthracene product.[24] This result showed again that it is not necessarily the same $Fe^{III}O(H)$ species that reacts with the substrate again after the initial H-atom abstraction reaction, but rather, the substrate radical may dissociate from the reaction cage to react with another $Fe^{IV}O$. This is different from enzymatic reactions where there is generally a single $Fe^{IV}O$ molecule per single turnover reaction.

There were also theoretical data that, now in hindsight, can be fit into the non-RM. The issue of the intermediate substrate radical being weakly bound to the heme iron-oxo complex (in case no enzyme residues hold it in place) was highlighted already in 2004.[22] The binding energy was found to be between 1.9-2.7 kcal mol^{-1}. If the dissociation entropy was taken into account, the binding may not necessarily have been favourable in terms of free energy. Similarly, in a study on the effects of counter ions on the self-interaction errors of DFT, the C-H

Learning Box 3

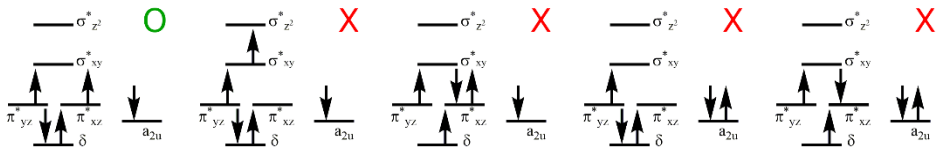

Fig. 2. Examples of different possible electron configurations in $S = 1/2$ $Por^{\bullet+}Fe^{IV}O$. The leftmost configuration is usually considered to be the lowest energy one. The four others are higher in energy and usually not obtained, but is attainable if the starting geometry is not good or if the calculation settings are not stringent.

Pitfalls in Calculations

DFT calculations provide valuable information about structure and energetics of molecules or their reactions. For running DFT calculations, it does not matter whether you are an experimentalist or a computational chemist. Similar to operating any other experimental equipment, one could learn to run his/her own computations after a proper training. However, the ability to analyse the results correctly provides the means to assess properly the reliability of the reported conclusions. In particular, when doing DFT calculations for reactive processes, understanding how electrons are migrating from one site to another during a chemical reaction is important. In a technical sense, this is because DFT calculations on open-shell systems do not always converge to the intended electronic state. Sometimes, an undesired, less stable electronic structure may be obtained (Fig. 2), and once this problem has surfaced, a new calculation must be submitted with a more decent initial orbital guess. Without such adjustments of the orbital guess, long calculations may just end up with producing wrong results, and worse yet, you may not even realise the problem! To avoid this sort of disappointment, the reader is advised to check the orbital occupancy frequently during calculations. Another important reason for having pictures of orbital occupancy is that, with electronic details in hand, you have a greater chance of being able to discuss the "chemistry" of the numbers produced by computers. For example, you may be able to explain why a particular structure or energy has been obtained by the DFT calculations. A key step towards gaining electronic details is to check how frontier orbitals are occupied by electrons. This can be done by analysing the Kohn-Sham orbitals or some sort of transformed orbitals such as natural orbitals, spin-natural orbitals or corresponding orbitals, using molecular graphics software. You may also check spin density (or population) distributions at atomic sites. The results of such orbital and spin analyses can be represented in a very concise form like Fig. 2, using bars and up/down arrows. Bars represent individual orbitals, and up and down arrows signify α and β electrons, respectively.

activation reaction of cyclohexane by the synthetic nonheme $[Fe^{IV}O(N4Py)]^{2+}$ species was investigated.[25] The dissociation free energy of the intermediate was also calculated to be substantially exothermic. Hence, the dissociation pathway would energetically be favourable compared to the rebound process, even though the rebound barrier was rather small.

There were also experimental results for species other than $Fe^{IV}O$ that were not compatible with the RM. For instance, synthetic nonheme $Ru^{IV}O$ species had also been extensively studied.[26–28] As the inorganic products were shown to be mostly Ru^{II} in the reactions studied, the suggested reaction mechanisms invariably included the rebound-type mechanism in the studies of C-H activation reactions by nonheme $Ru^{IV}O$ species. However, Ru^{III} species were observed from time to time, together with a sizeable mixture of multiple organic products.[27,29] This has prompted proposals of complicated simultaneous reaction pathways, one of them being a non-rebound type pathway.[27,28] More recently, in a study with $[Mn^{n+}O(H_3buea)]^{(n-5)+}$ (n = 3 or 4, $[H_3buea]^{3-}$ = tris[(*N*′-*tert*-butylureaylato)-*N*-ethylene]aminato) reacting with 1,2-diphenylhydrazine,[30] azobenzene was observed as a product. This reaction resulted in formation of the corresponding $Mn^{III}OH$ species, and not Mn^{II} as would have been expected in a catalyst:substrate 1:1 stoichiometry reaction. However, it was not possible to derive the reaction stoichiometry itself from the given reaction concentrations.[30] Another study combining theory and experiment used three different ligands (tetraphenylporphyrin, a salen-type ligand, and terpyridine) to investigate the competition of hydroxylation versus desaturation reactions in Mn-oxo species.[31] Usage of radical scavengers, such as CCl_3Br or *N*-bromosuccinimide, did not affect the reaction, ruling out a free radical dissociation mechanism and thus supporting a rebound/desaturation reaction. However, since these experiments were done under aerobic conditions, where O_2 itself might act as a radical scavenger (indeed, the product yields were different in anaerobic conditions), and combined with the low overall product yield, a dissociation mechanism might operate in this case.

Even with metal oxidation states other than IV, there are examples of reactions that may not utilize the RM. Using the manganese di-oxo species $[Mn^{V}(O)_2(TF_4TMAP)]^{3+}$ (TF_4TMAP = *meso*-tetrakis(2,3,5,6-tetrafluoro-*N*,*N*,*N*-trimethyl-4-aniliniumyl)porphyrinato dianion) in the reactions with substrates with weak C-H bonds, no rebound products were formed, even though an initial H-atom abstraction reaction was confirmed by a good correlation between the rates and the C-H bond strengths as well as large KIE values.[32] These reactions were performed in aerobic conditions and through ^{18}O labelling, it was confirmed that atmospheric O_2 interferes with the reaction. Moreover, a $[(OH)Mn^{IV}O(TF_4TMAP)]^{3+}$ product was detected instead of $[Mn^{III}O(TF_4TMAP)]^{3+}$; the formation of the latter species would have been expected if a two-electron reduction reaction (e.g., a product from RM) would occur. As TF_4TMAP is a porphyrin ligand, these results hint at the possibility that the metal type, its oxidation numbers and the available spin states are far more important than the specific ligand type for their rebound barriers.

Learning Box 4

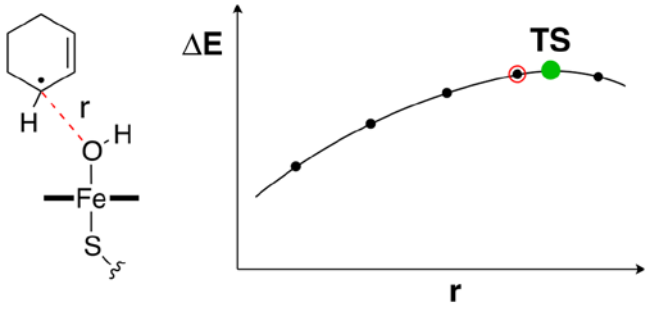

Fig. 3. Schematic drawing of the TS for a rebound step. The reaction of cyclohexene is depicted as an example.

Transition State Search

When optimizing the TS geometry for a rebound step, you can first scan the energy surface. In doing so, you may use the distance between C and O ("r") in Fig. 3 (left) as the reaction coordinate. More specifically, you may use a series of different r values, and at each distance, r is fixed and the remaining internal coordinates are relaxed. As a result, a specific r value can be found at which the energy is maximum (highlighted by a red circle). Using this maximum-energy point as an initial geometry, further geometry optimization may be performed so that the geometry is located precisely at the saddle point of the energy surface. This TS optimization may be followed by a harmonic frequency calculation at the same DFT level. If the geometry optimization has been successful, your imaginary frequency should contain large stretching motions of the carbon and oxygen atoms in the direction of the newly formed C–O bond.

The first study that questioned the RM pathway while establishing a non-RM pathway utilized nonheme $Mn^{IV}O$ species,[33,34] followed by the study of $Fe^{IV}O$ species with the same ligands.[35] These studies combined all the tell-tale signs indicated so far, supplemented with computational results. Similar studies were also performed with $Cr^{IV}O$, $Fe^{V}O$ and $Ru^{IV}O$ species (*vide infra*),[36–38] and others are currently in progress. As we indicated in the Introduction section, understanding the second (rebound) barrier holds the key to the mechanistic identification of a RM vs. non-RM. This part of the reaction is a fast process, usually not rate-limiting, and difficult to characterize fully with experimental methods. The best characterisation therefore comes from theoretical methods, which is the focus of this review. Learning Boxes 3 and 4, together with Figs. 2 and 3, detail practical hands-on tips in approaching this subject via theoretical methods. Hence, we will first describe below a theoretical orbital view of the reactions at hand, particularly for the Cpd I case, where there is a RM, before moving on to the cases of nonheme non-rebound species studied so far.

3. Orbital discussions

3.1 Ground state $Fe^{IV}O$ orbital configurations

To gain insights into the reaction mechanism, we must first understand the electronic structure of the active species. Fig. 4 shows the high-lying valence orbitals for the metal-oxo species in the cases of a) a porphyrin-type ligand (as in P450), b) a nonheme ligand with a trigonal bipyramidal geometry (as in TauD) and c) a nonheme ligand with an octahedral geometry (as in many synthetic complexes). In the current description, we focus on the electronic configurations of $Fe^{IV}O$ species, but the orbitals themselves are applicable to other metal-oxo systems as well.

The electronic population for the porphyrin ligand can be described as either a ferryl $Fe^{IV}O$, or a perferryl $Fe^{V}O$ equivalent (so called Cpd I in P450, which is a $Por^{+\bullet}Fe^{IV}O$ species). Thus, the FeO moiety possesses two identical-spin electrons in the $\pi^*_{xz/yz}$ orbitals made from the Fe(3*d*) and O(2*p*) atomic orbitals of the FeO moiety (see Learning Box 5), by analogy to the triplet dioxygen molecule. In the P450 $Por^{+\bullet}Fe^{IV}O$ species in Fig. 4a, the porphyrin macrocycle is in a radical cation state and an unpaired electron resides in the "a_{2u}" type orbital. Since the spins of the $\pi^*_{xz/yz}$ and a_{2u} electrons are very weakly coupled, these complexes can have two closely lying states, $S = 1/2$ and $S = 3/2$.[2] In P450 and its analogues (e.g., chloroperoxidase), the lower state is $S = 1/2$, whereas in synthetic models the lower state is by and large $S = 3/2$.

In nonheme enzymes and some of the known synthetic complexes, where the coordination sphere is thought to be trigonal bipyramidal, the *d*-block orbitals of the $Fe^{IV}O$ complex contain two more unpaired electrons such that the ground state of the complex is quintet with a spin quantum number $S = 2$ (Fig. 4b).[39] In the majority of synthetic $Fe^{IV}O$ complexes, where the ligand coordination sphere is usually octahedral, this state lies several kcal mol^{-1} higher than the $S = 1$ state, wherein only the $\pi^*_{xz/yz}$ orbitals are singly occupied with identical spin electrons (Fig. 4c).

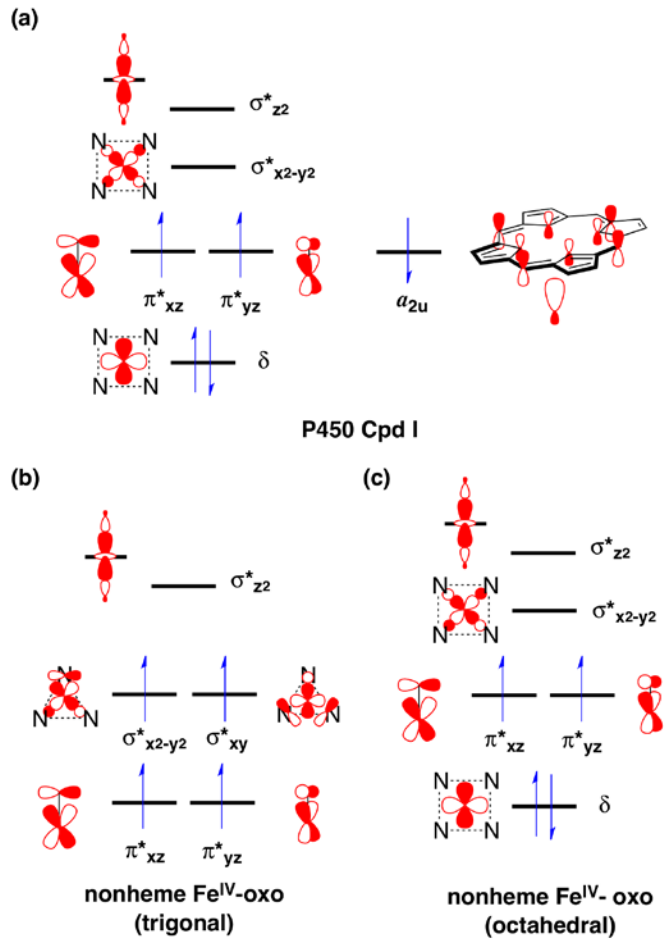

Fig. 4. a) The $S = 1/2$ electronic structure of a $Por^{+\bullet}Fe^{IV}O$ complex. In the energetically degenerate $S = 3/2$ state, the a_{2u} electron has an α-spin. b) Nonheme $Fe^{IV}O$ complex with a trigonal bipyramidal coordination sphere, where $S = 2$ is the usual ground state. c) Nonheme $Fe^{IV}O$ complex with an octahedral coordination sphere, where $S = 1$ is the usual ground state.

3.2 Electron shift diagrams during rebound for P450

In P450-catalyzed alkane hydroxylation reactions, H-atom abstraction (first step) results in a shift of a hydrogen atom from the alkane substrate to P450 Cpd I. Thus, there is a net shift of one proton and one electron, thereby leading to the formation of a $PorFe^{IV}OH$-type intermediate, which is frequently referred to as Compound II (Cpd II) in P450 (although sometimes denoted as $PorFe^{IV}O$, differing by H^+). A slight deviation from this description is seen in the same intermediate in the $S = 5/2$ state, where calculations have shown that it may be better described as the isoelectromer $Por^{+\bullet}Fe^{III}OH$.[40] In the rebound step (second step) of alkane hydroxylation, the substrate radical attacks the hydroxyl moiety of the Cpd II species to form a new C–O bond. The energy barrier for this second step depends on the spin state (see Introduction), and the reaction pathway can be different depending on this energy barrier, including a possible non-RM. It is therefore useful to understand how the orbitals and their electron occupations vary during this process.

Fig. 5 compares the electron occupation patterns of the Cpd II intermediate in the doublet ($S = 1/2$), quartet ($S = 3/2$), and sextet ($S = 5/2$) spin states. This reaction has earlier been described to be attended by a second electron shift process from the substrate to the π* or $\sigma^*_{z^2}$ orbitals, which served as a simple and intuitive picture explaining the reaction.[40] Hence, for instance in the doublet state, the substrate $\phi_{C\bullet}$ orbital starts the

Fig. 5. Occupations and electron shift patterns for the initial phase of the rebound step in P450 reactions. Blue arrows represent the electrons that originate from the substrate. In the $S = 1/2$ state, the electron in the substrate radical $\phi_{C\bullet}$ orbital shifts to π^*_{yz} orbital in a reaction without a barrier. In the $S = 3/2$ state, the electron shift is to the $\sigma^*_{z^2}$ orbital, which is higher in energy than π^*_{yz} and may contribute to the small rebound barrier seen in this spin state. In the $S = 5/2$ state, the electron shift is to π^*_{yz}, but a small barrier is still seen, possibly due to a different oxidation state in the FeOH moiety compared to the other spin states (III vs. IV). Also, an extra step here is to move the α-electron in π^*_{yz} to the lower-lying orbital a_{2u}.

Learning Box 5

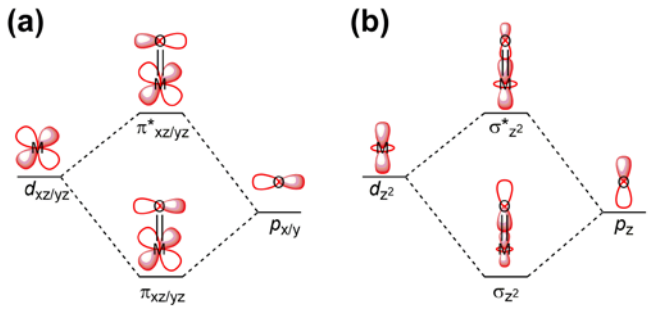

Fig. 6. Examples of combining a *d*-orbital on a metal (M) with a *p*-orbital on monooxygen (O) when forming an MO species. a) The d_{xz} or d_{yz} orbital combines with p_x or p_y to form the bonding orbitals π_{xz} or π_{yz} and the anti-bonding orbitals π^*_{xz} or π^*_{yz}. b) Similarly, other metal *d*-orbitals combine with other oxygen *p*-orbitals, here shown for metal d_{z^2} combining with p_z on the oxygen atom to form the bonding orbital σ_{z^2} and the anti-bonding orbital $\sigma^*_{z^2}$ (see ESI Fig. S1 for a full picture). Because of the d_{z^2} dominance in the latter orbital, it is considered colloquially to be one of the *d* orbitals in the *d* block. This convention is convenient for tracking oxidation states. The above conceptual pictures naturally hold for the reverse reaction as well, i.e. M-O bond breaking reactions.

The "*d*-orbitals" of Metal-Oxo Species

A colloquial conception among experimentalists and theoreticians alike is that there are five *d*-orbitals in metal-oxo systems, analogous to the five *d*-orbitals in the isolated metal atom. This is not technically correct as the five *d*-orbitals in the metal interact with the *p*-orbitals of the oxygen atom as well as the ligand atoms, creating new hybrid orbitals (see Fig. 6 for examples). Fortunately, only the top five of these hybrid orbitals are high enough in energy to be relevant in simple reactions, e.g. hydrogen atom transfers, rendering the five *d*-orbital concept intact, such as in Fig. 4. Occasionally however, more than the top five orbitals are required to properly describe a system, such as in the case of a S = 5/2 $Mn^{IV}O$ species,[34] where a bonding π orbital is singly occupied. The formally stringent view should therefore be that rather than five *d*-orbitals in a metal-oxo system, there are hybrid orbitals derived from the five *d*-orbitals of the isolated metal atom. In the case of a tetragonal pyramidal or octahedral structure, there are nine such hybrid orbitals, as shown in ESI, Fig. S1. However, the five *d*-orbitals concept remains extremely useful as it in most cases allows oxidation state determination of the metal centre easily, and hence also the "number of *d* electrons" left on the metal.

second step rebound reaction by donating an electron to the π^*_{yz} orbital, which changes the number of electrons at the iron centre from 4 to 5. Thus, the formal oxidation state of iron changes from IV to III. The rebound step in the quartet state reaction occurs along the same line (Fig. 5, centre); however, the $Fe^{IV}O$ orbital that is involved in this reaction is different. The substrate electron goes from $\phi_{C\bullet}$ to the $\sigma^*_{z^2}$ orbital, which is higher in energy than π^*_{yz}. Although this electron shift increases the number of unpaired electrons on iron from 2 to 3, which may give rise to some degree of exchange stabilization,[41] the destabilizing effect of interacting with a high-lying orbital ($\sigma^*_{z^2}$) slightly surpasses the exchange stabilization. As a result, there is usually a small yet nonzero rebound barrier in the quartet state, whereas no barrier is usually observed for the pathway in the doublet state. This distinction has been utilized to provide an explanation for the too short apparent lifetime of the radical intermediate in a P450 reaction, obtained experimentally for radical clock substrates.[42,43]

A nonzero barrier is also obtained computationally for the rebound step in the sextet state.[40] One possible reason for the existence of a rebound barrier here may be that the oxidation state of the iron is formally III in the Cpd II intermediate stage, in comparison to IV in the doublet and quartet states. Thus, when the rebound process is taking place, there may be additional electron repulsion between the substrate and the $Fe^{III}OH$ site, compared to the other spin states. This spin state also requires an ensuing electron transfer step from the π^*_{yz} orbital to the singly occupied, lower-energy a_{2u}.

The same orbital interaction patterns as described in Fig. 5 also apply to the ring-closure step of olefin epoxidation, which is another very important reaction that P450s can catalyse. It should be noted, however, that a rebound step is not obtained

Learning Box 6

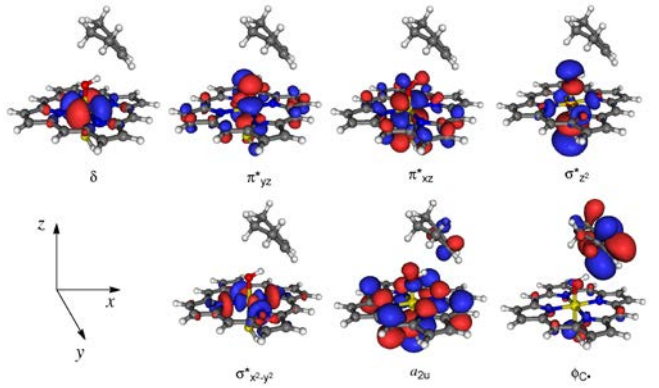

Fig. 7. Key orbitals for the H-abstracted intermediate in the reaction between P450 Cpd I and cyclohexene.

Orbitals and Geometry Information

The shapes of the orbitals are not just mathematical curiosities, but they also provide important information about the interaction geometries in reactions. In Fig. 7, we define the Fe-O direction the as z-axis and the projected O-H direction perpendicular to z as the x-axis. We can then see that one component of the π^*_{yz} orbital is the p_y orbital on O. Hence if the substrate orbital $\phi_{C\bullet}$ interacts with π^*_{yz}, an Fe-O-C angle of 90° would lead to maximum overlap (actually, due to steric hindrance as well as to avoid the node in the latter orbital, the maximal overlap occurs at larger angles, ca 120°) between the orbitals from the O and C. Similarly, if $\phi_{C\bullet}$ instead interacts with $\sigma^*_{z^2}$, maximum overlap occurs at the Fe-O-C angle of 180°. Hence, measuring the Fe-O-C angle can provide important information about orbital interactions. We can also see that due to the fact that δ, σ^*_{xy} and a_{2u} orbitals are have little or no delocalization on O, they are not likely to interact directly with $\phi_{C\bullet}$.

for other types of reactions such as sulfoxidation and *N*-oxidation. These reactions are completed in one step.

3.3 Orbital reorganisation during rebound for P450

The initial electron shift as described above is useful for understanding the electron movements during the rebound reaction. However, while accounting for changes in the metal oxidation state, this picture does not reveal the bond making/breaking aspect of the reaction. For instance, Fig. 5 does not account for the fact that once the Fe-O bond is broken after the rebound step, the orbitals on Fe are predominantly atomic *d*-orbitals (and not π or σ, Fig. 6). Also, the figure shows only seven valence electrons in motion, using only six valence electron orbitals on the PorFeO moiety. This leaves at the end of the reaction a correct electron account corresponding to the $PorFe^{III}$ product species on the catalyst side, but not on the substrate side. It is therefore important to understand how the orbitals are changing during the reaction concomitantly with the electron shift. In this section, we describe the above process more generally as an interaction between the orbitals in order to account for the whole reaction (including the rebound motion itself) with a proper electron count.

At the Cpd II intermediate stage, the substrate $\phi_{C\bullet}$ orbital needs to overlap with FeOH orbitals in order to initiate the electron shifts. In the *S* = 1/2 state, the overlap is with the π^*_{yz} orbital, in an ideal Fe-O-C attacking angle of 90° (see Learning Box 6 and Fig. 7).[39] However, overlap with π^*_{yz} orbital also means that overlap with its low-energy bonding correspondent π_{yz} would be geometrically possible too. As a result of this mixing, the Fe-O bond elongates. This leads to π_{yz} and π^*_{yz} collapsing and separating into their constituent orbitals d_{yz} on the iron and p_y on O (see Fig. 6a). At the same time, the forming p_y orbital combines with the substrate $\phi_{C\bullet}$ orbital to form a bonding $\sigma_{C\text{-}O}$ and anti-bonding $\sigma^*_{C\text{-}O}$ orbital (Fig. 8a). The $\sigma^*_{z^2}$ and π^*_{xz} orbitals also break down to their constituent orbitals, ending up as *d*-orbitals on Fe and lone-pair orbitals on O (ESI, Fig. S2).

Similarly, the substrate $\phi_{C\bullet}$ orbital in the *S* = 3/2 state now interacts with the σ_{z^2} and $\sigma^*_{z^2}$ orbitals, where these σ orbitals break down into d_{z^2} on Fe and p_z on O (Fig. 6b), leading to the same C-O bonding and anti-bonding orbitals in its interaction with $\phi_{C\bullet}$ (Fig. 8b). This interaction occurs through an ideal Fe-O-C interaction angle of 180°. The *S* = 5/2 state has an identical orbital interaction as in the *S* = 1/2 state.

Thus, the above description of the well-studied Cpds I and II orbital interactions gives us a reference point for further comparisons with nonheme systems. Specifically, the interacting high-energy orbitals and electron repulsions during the second step was identified as possible reasons to why this step has a barrier in the higher spin states, as opposed to no barrier in the *S* = 1/2 state. This issue is revisited later on in the context of nonheme species and the non-RM.

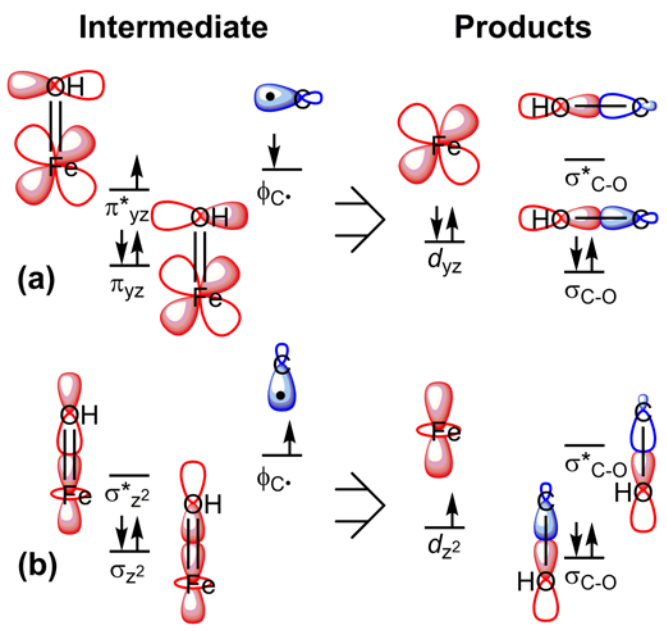

Fig. 8. The "before" and "after" pictures of key orbitals in the rebound step of P450 reactions, with conserved electron count. The substrate radical $\phi_{C\bullet}$ interacts with either the (a) π_{yz}/π^*_{yz} or (b) $\sigma_{z^2}/\sigma^*_{z^2}$ orbitals to form the C-O bonding orbital $\sigma_{C\text{-}O}$ (consisting of $\phi_{C\bullet}$ and one *p* orbital from O) and the corresponding *d* orbital on Fe.

4. Studies on non-rebound mechanism

4.1 $Mn^{IV}O$

The first conclusive study exploring the possibility of a non-RM preference over the RM explicitly was done using $[Mn^{IV}O(Bn\text{-}TPEN)]^{2+}$.[33] The reaction of $[Mn^{II}(Bn\text{-}TPEN)]^{2+}$ with PhIO afforded the formation of an *S* = 3/2 $[Mn^{IV}O(Bn\text{-}TPEN)]^{2+}$ species. This $Mn^{IV}O$ complex was found to be highly reactive. For instance, the second order rate constant for C-H activation of cyclohexane was $3.3\bullet10^{-3}$ M^{-1} s^{-1} at 25 °C, in comparison with $3.9\bullet10^{-4}$ M^{-1} s^{-1} at the same temperature for $Fe^{IV}O$ with the same ligand and substrate, albeit in different solvent conditions. Again, the rate-limiting H-atom abstraction step was established by showing a linear correlation between the reaction rates and C-H bond strengths as well as a large KIE value (7.9). Also here, the total product yield was low, as exemplified by the reaction with ethylbenzene which gave the following yields: 1-phenylethanol 23%, acetophenone 12%, and styrene 7%. Considering that acetophenone requires twice the oxidizing equivalents of the others, the total product yield based on catalyst used was about 54%. The oxygen atom in the products originated from the $Mn^{IV}O$ species, as proven by ^{18}O labelling in anaerobic environment. In addition, the inorganic product was Mn^{III}, as verified by ESI-MS, EPR and XAS. A control reaction carried out with a mixture of the corresponding $Mn^{IV}O$ and Mn^{II} species did not produce Mn^{III}, thus ruling out a possibility of a comproportionation reaction. In contrast to the C-H activation reactions, sulfoxidation with $Mn^{IV}O$ resulted in the formation of a Mn^{II} product, supporting that the Mn^{III} species was not the product resulting from a comproportionation reaction between $Mn^{IV}O$ and Mn^{II} species.

The experimental observation was followed by theoretical studies of both $[Mn^{IV}O(Bn\text{-}TPEN)]^{2+}$ and $[Mn^{IV}O(N4Py)]^{2+}$ in the oxidation of cyclohexane.[34] Compared to $Fe^{IV}O$ (*vide infra*), $Mn^{IV}O$ was found to have a larger number of possible valence

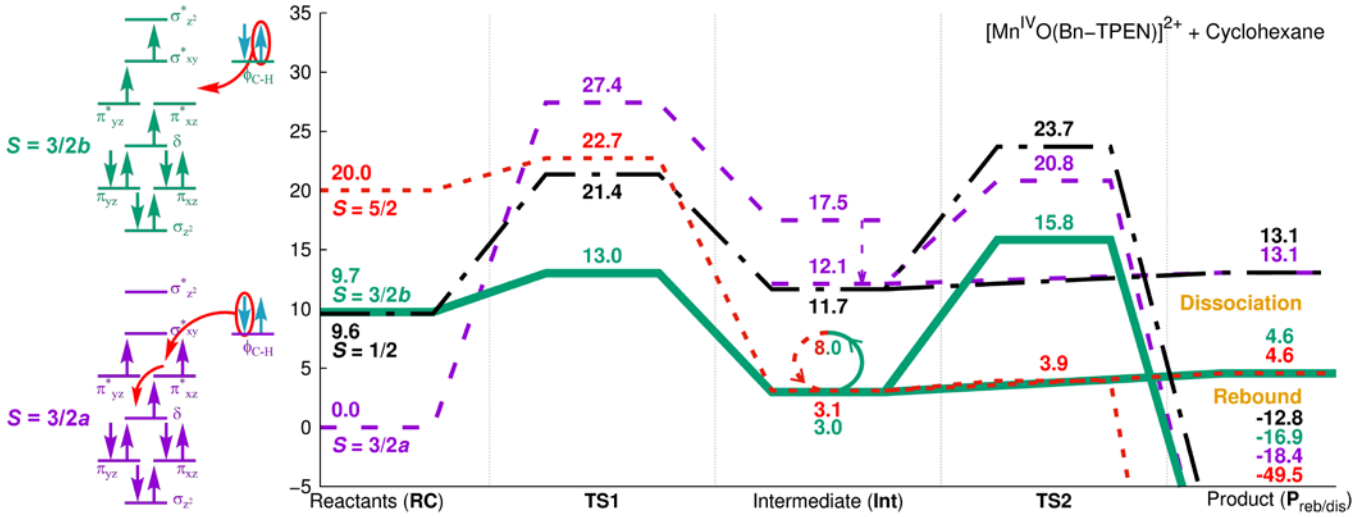

Fig. 9. Two S = 3/2 valence electron configurations of $Mn^{IV}O$ was found during the C-H activation and rebound reaction. The ground state S = 3/2*a* was in fact found to lead to a high rate-limiting barrier, while the excited state configuration S = 3/2*b* was found to have the overall lowest rate-limiting barrier (left).[34] At the intermediate step, the energetically lowest states are the S = 3/2*b* and S = 5/2 states. The conversion from S = 3/2*b* to 5/2 involve a spin state shift on the free substrate radical, which is not believed to occur faster than corresponding to a minimum barrier of 5 kcal mol^{-1} (symbolized by a loop in the center).[34] Hence, the most probable route after the S = 3/2*b* H-atom abstraction is the dissociation of the free substrate radical, featuring only 1.6 kcal mol^{-1} in dissociation energy. See ESI, Fig. S3 for corresponding orbital occupation diagrams for all the $Mn^{IV}O$ states, as well as for the $Fe^{IV}O$ reactions. Figure adapted from ref. [34].

electron configurations. Furthermore, a detailed understanding of these electron configurations was necessary to explain the C-H activation reaction correctly. Two of the possible valence electron configurations of $Mn^{IV}O$ are depicted in Fig. 9. The *z*-axis is defined along the Mn-O bond, and eight valence orbitals in the $Mn^{IV}O$ moiety are included and denoted σ_{z^2}, π_{xz}, π_{yz}, δ, π^*_{xz}, π^*_{yz}, σ^*_{xy} and $\sigma^*_{z^2}$. The *x*-axis is selected here to coincide with the projected MnO-HC direction when a C-H activating substrate (cyclohexane) was present. In the study, two different S = 3/2 states were found to be relevant to the initial H-atom abstraction step. One had δ, π^*_{xz}, and π^*_{yz} orbitals singly occupied (configuration *a*), while the other one (configuration *b*) had an empty π^*_{xz} orbital with a singly occupied σ^*_{xy} orbital instead. The former configuration was overall lowest in energy (lower by 9.7 kcal mol^{-1} than *b*, in the case of $[Mn^{IV}O(Bn\text{-}TPEN)]^{2+}$) and deemed to be the ground state at the reactant stage. At the TS, however, configuration *b* was found to have the lowest energy TS at 13.0 kcal mol^{-1}, far lower than 27.4 kcal mol^{-1} for configuration *a* (Fig. 9). It is also worth noting that the second lowest TS was found for the S = 1/2 state at 21.4 kcal mol^{-1}. Hence, if the assumption had been made that there should be only one reactive S = 3/2 state, it would have led to the conclusion that the S = 1/2 state had the lowest energy barrier. The above results show that we instead have an excited state reactivity, underscoring the need of properly following the electron movements during the reaction (see Learning Box 3). This reaction was the rate-limiting step, leading to an overall energetically lowest intermediate which was connected to the S = 3/2*b* state.

Although the rate-limiting step should be used for a fair comparison of the computationally and experimentally derived reaction rates, it is actually in the second step that the choice of pathways between rebound, desaturation or dissociation is made. For all examined spin states, it was found that the dissociation energy was at most 1.6 kcal mol^{-1} (Fig. 9, this value did not include the dissociation entropy, which would inevitably lower this value further). To compete with this, the rebound or desaturation barriers must be less than that. It was found that only the S = 5/2 state had a low rebound barrier enough to compete with this (0.8 kcal mol^{-1}). However, as the S = 5/2 state was high in energy at both the reactant and TS states, most probably the S = 5/2 state has to be attained at the intermediate state from another spin state. If we assume that this happens from the energetically lowest state (S = 3/2*b*, Fig. 9), then the β-spin on the substrate has to flip to obtain the overall S = 5/2 state. While this event is assumed to be fast, it is doubtful that it will be faster than the dissociation (1.6 kcal mol^{-1} would correspond to 10^{11} s^{-1} in rate at room temperature). The process will be inevitably more complex if switching to the S = 5/2 state from any of other states; hence the final conclusion is that dissociation is a more likely path than rebound, desaturation or spin state shifts.

These results led to the formulation of the non-RM shown in Fig. 10. After the H-atom abstraction step, the substrate radical dissociates, leaving behind the $Mn^{III}OH$ species as the inorganic product. The substrate radical then reacts with a second $Mn^{IV}O$ complex, which through solvent exchange results in the hydroxylated substrate and again a Mn^{III} product. Essentially, a two electron reduction reaction, whereby Mn^{IV} was thought to be converted to Mn^{II} through the rebound reaction, is now explained instead in terms of reductions of two

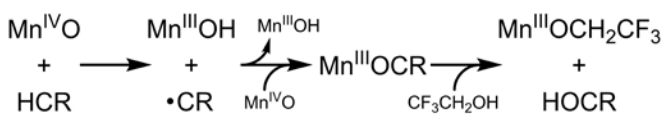

Fig. 10. Proposed 2:1 catalyst:substrate stoichiometric hydroxylation reaction mechanism involving substrate dissociation and solvent binding steps.

Mn^{IV} species into two Mn^{III} species, and this rationale is compatible with the experimental and theoretical results.

4.2 $Fe^{IV}O$

A case study involving C-H activation reactions with $[Fe^{IV}O(Bn\text{-}TPEN)]^{2+}$ and $[Fe^{IV}O(N4Py)]^{2+}$ was conducted in order to investigate the non-RM.[35] The experimental results were similar to what has been seen in the $Mn^{IV}O$ case. Using a wide range of substrates (9,10-dihydroanthracene, 1,4-cyclohexadiene, triphenylmethane, ethylbenzene and cyclohexane), Fe^{II} was seen only in small amounts among the products. For instance, the reaction of $[Fe^{IV}O(Bn\text{-}TPEN)]^{2+}$ with ethylbenzene yielded only 10% of $[Fe^{II}(Bn\text{-}TPEN)]^{2+}$ as a product, although $[Fe^{IV}O(Bn\text{-}TPEN)]^{2+}$ disappeared completely. Adding an electron donor, ferrocene, to the resulting solution increased the amount of $[Fe^{II}(Bn\text{-}TPEN)]^{2+}$ to 100% with 90% formation of ferrocenium ion. Similar results were obtained with $[Fe^{IV}O(N4Py)]^{2+}$. To investigate the possibility of Fe^{III} formation through a comproportionation reaction, equal amounts of $[Fe^{IV}O(N4Py)]^{2+}$ and $[Fe^{II}(N4Py)]^{2+}$ were mixed, but no formation of Fe^{III} species was observed, ruling out a comproportionation reaction. Further, the identities and ratios of the organic products were different depending on the reaction conditions. In anaerobic conditions in CH_3CN solution, $[Fe^{IV}O(Bn\text{-}TPEN)]^{2+}$ yielded 16% C-H activation products when reacting with cyclohexane at 25 °C, with the majority product being cyclohexanol. Usage of $[Fe^{IV}(^{18}O)(Bn\text{-}TPEN)]^{2+}$ resulted in almost 100% abundance of ^{18}O in cyclohexanol. In aerobic conditions, however, this number was only 23% and the majority product here was cyclohexanone. This indicates that O_2 interfered the reaction, supposedly at the intermediate stage, by reacting with the substrate cyclohexanyl radical. A similar result was obtained when CCl_3Br was used in anaerobic conditions; the only product detected was bromocyclohexane which indicated a reaction of CCl_3Br with the cyclohexanyl radical.

In the same study, DFT calculations were performed in order to support the experimental conclusions (see ESI, Fig. S3 for orbital occupation diagrams). The reactant was found to be in the $S = 1$ state, as verified both experimentally and theoretically in earlier studies.[44,45] Using cyclohexane as substrate, the ensuing reactions were, however, lower in energy at the $S = 2$ state, due to the stronger exchange enhancement that arises from the interactions between unpaired electrons of the same spin.[41] It was therefore presumed here, as well as in most other studies in this field, that a spin flip can occur to utilize this low energy pathway, depending on the spin-orbit coupling interaction between the two spin states. The exact calculations of the spin-orbit coupling interactions and the corresponding spin flip probabilities are time consuming and are not practically feasible for the current system. Nevertheless, it turns out that the conclusions of this study would not be changed even if the reaction were to occur in the $S = 1$ state. Hence, while the values of the $S = 2$ state reactions were presented, the mechanistic issue was independent of the exact nature of the reactive spin state.

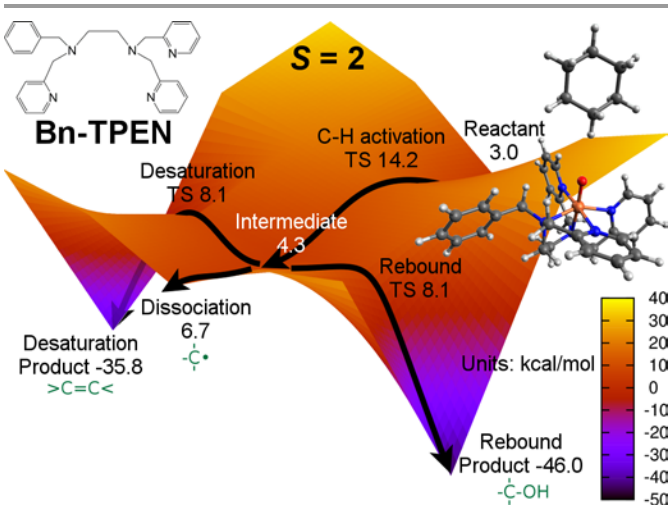

Fig. 11. DFT calculated $S = 2$ potential energy surface of the C-H activation reaction of cyclohexane by $[Fe^{IV}O(Bn\text{-}TPEN)]^{2+}$. The rebound and desaturation barriers are both at 8.1 kcal mol^{-1}, which is higher than the energy of the substrate radical dissociated state (6.7 kcal mol^{-1}). Adapted from ref. [35].

The initial H-atom abstraction was found to be the rate-limiting step with a barrier height of 14.2 kcal mol^{-1} in the $S = 2$ state for $[Fe^{IV}O(Bn\text{-}TPEN)]^{2+}$ (Fig. 11). The second step featured a rebound barrier of 8.1 kcal mol^{-1}, and incidentally, the same barrier height for the desaturation reaction was obtained. Note that this value is relative to the $S = 1$ reactant and would be even lower relative to the $S = 2$ intermediate point (3.8 kcal mol^{-1}). Thus, these reactions are entirely possible, given that the barriers for the second step is low and that the reaction just had gone through a rate-limiting H-atom abstraction step with an even higher energy barrier. However, the dissociation energy, calculated as the energy difference between the intermediate complex and the hypothetical state in which the substrate radical intermediate is placed 20 Å away from $Fe^{III}OH$, is less than the other barrier heights (2.4 kcal mol^{-1}). A simple explanation for this is that there is nothing that anchors the substrate radical to the catalyst, such as hydrogen bonds or steric restrictions. There are also two other factors that could enhance the preference for dissociation. One is that the dissociation entropy would certainly favour this process even more. Second, given that the cyclohexane substrate has a relatively strong C-H bond, it can be assumed that its C-O bond would be relatively strong as well. Hence, using any other substrate, which is likely to have weaker C-H bonds, the rebound product energy would be less exothermic than in the cyclohexane case. According to the Bell-Polanyi-Evans principle,[46,47] this should lead to a higher rebound barrier height as well, and dissociation would be even more preferred. The cyclohexane case is therefore likely to constitute a scenario in which the dissociation is preferred over the rebound by a minimal margin. However, since triphenylmethane with a weak C-H bond shows evidence of a rebound reaction,[23] it is clear that this is not an absolute rule, and other factors need also to be taken into account on a case by case basis.

Nevertheless, the experimental observations, such as the low organic product yield (less than 50%), the formation of Fe^{III} instead of Fe^{II} as an inorganic product, the interference of O_2

and CCl_3Br with the reaction process, and the energetic considerations through DFT calculations all point to a process where the RM seems to be disproved in the studied system. This shows that detecting alcohol products alone is not sufficient to prove a rebound process, and alternative pathways must be considered. A plausible pathway is similar to what has been described above for $Mn^{IV}O$. After the initial C-H activation, a dissociation event results in a reaction with a second $Fe^{IV}O$ to form Fe^{III} species.

4.3 $Cr^{IV}O$

In order to investigate the non-RM with $Cr^{IV}O$ species, a Cr(III)-superoxo complex, $[Cr^{III}(O_2)(TMC)Cl]^+$, was prepared by bubbling O_2 into a solution of $[Cr^{II}(TMC)Cl]^+$. Addition of PPh_3 to the solution of $[Cr^{III}(O_2)(TMC)Cl]^+$ caused an oxygen atom transfer to PPh_3, resulting in the formation of $[Cr^{IV}O(TMC)Cl]^+$.[48] This $Cr^{IV}O$ species was then studied for C-H activation reactions with cyclohexadiene, xanthene and dihydroanthracene, affording the formation of benzene (43% yield), xanthone (45%) and anthracene (42%), respectively.[36] The inorganic product detected here was shown to be $[Cr^{III}OH(TMC)(Cl)]^+$, and ^{18}O labelling experiment established that the oxygen atom in the products derived from $Cr^{IV}(^{18}O)$.

The ~50% organic product yields indicate that the desaturation reactions were seemingly performed under 2:1 catalyst:substrate stoichiometric conditions. The formation of Cr^{III} species as a product reinforces the likelihood that a dissociation reaction takes place after the initial H-atom abstraction, which is then followed by desaturation by a second $Cr^{IV}O$ complex. The scenario, derived from the DFT calculations, is in fact clearer for this issue than for the corresponding Mn and Fe cases. The reactant ground state is theoretically found to be the S = 1 state, which is in agreement with experiments. The initial H-atom abstraction reaction from cyclohexadiene was found to occur with a lowest barrier of 15.8 kcal mol^{-1} in the S = 1 state, indicating that no spin state changes are occurring. While the dissociation energy is less than 1 kcal mol^{-1} at the intermediate stage, the rebound and 1:1 desaturation reactions have barriers that exceed 20 kcal mol^{-1}, clearly implicating a dissociation mechanism.

4.4 $Fe^{V}O$

Given that the dissociation reaction is possible due to a weak interaction between the catalyst and the substrate radical, it is plausible that other types of metal-oxo species could prefer the dissociation mechanism. This appears to be the case with the $[Fe^{V}O(TAML)]^-$ (TAML = 3,3,6,6,9,9-hexamethyl-3,4,8,9-tetrahydro-1H-1,4,8,11-benzotetraazacyclotridecine-2,5,7,10(6H,11H)-tetraone) complex.[37,49,50] The pattern observed here is similar to that for other $M^{IV}O$ species described above. Using ethylbenzene as substrate, analysis of the products revealed the formation of 1-phenylethanol (38%) and styrene (12%) under an Ar atmosphere. Bromocyclohexane was obtained as the sole product when cyclohexane was used as substrate and CCl_3Br was present. The inorganic product was $[Fe^{IV}O(TAML)(m\text{-CBA})]^-$ as indicated by ESI-MS and EPR. Also, adding ferrocene resulted in the formation of an Fe^{III} species as well as ferrocenium ion (85% yield), strongly supporting the presence of Fe^{IV} in the solution.[37] As expected, DFT calculations resulted in all the rebound energy barriers being higher than the dissociation barrier.

4.5 $Ru^{IV}O$

Very recently, a non-RM of a $Ru^{IV}O$ species has been investigated in C-H activation reactions;[38] unlike many of the earlier experiments,[26–29] the investigated complex, $[Ru^{IV}O(terpy)(bpm)]^{2+}$ (terpy = 2,2′:6′,2′′-terpyridine, bpm = 2,2′-bipyrimidine), yielded a stable Ru^{III} species instead of Ru^{II}. Hence, in the reactions with both ethylbenzene and cyclohexene, the usual tell-tale signs, such as the <50% product yields, the interference of O_2 and CCl_3Br during the reaction, and the formation of Ru^{II} products resulting from non-C-H activation (i.e. epoxidation or sulfoxidation) reactions, were found. DFT calculations supported this view, showing that the dissociation energy for the radical intermediate is less than the rebound/desaturation barriers. In fact, while the usual rebound/desaturation barriers for other metal-oxo species are moderate (but still not competitive with dissociation), in this $Ru^{IV}O$ species, these barriers were clearly not competitive (above 26 kcal mol^{-1} using ethylbenzene) without spin state changes. Even when a spin state change was taken into account, the dissociation was still favourable by 2.9 kcal mol^{-1} over the rebound barrier.

5. Heme vs. nonheme $Fe^{IV}O$ species

An interesting discussion is about the decisive factor that makes the nonheme systems prefer the dissociative pathway, as opposed to the case of $Por^{+\bullet}Fe^{IV}O$ species, where the rebound reaction is well established. As discussed above, the second (rebound) barrier is the key for the determination of the reaction pathways. In essence, a low dissociation energy should be a general feature regardless of metal or ligands as long as there are no binding factors involved at the intermediate stage, such as hydrogen bonds or binding residues as in enzymes. Therefore, to compete with such a low dissociation energy, the rebound process must be *de facto* barrierless. Calculations have shown that this is indeed the case with S = 1/2 $Por^{+\bullet}Fe^{IV}O$.[2] The fact that the S = 3/2 state has a nonzero barrier supports this proposal, as it is postulated to hydroxylate rearranged radical clocks.[2] In biomimetic reactions, the S = 3/2 state may proceed via the non-RM pathway. What causes this odd behaviour of $Por^{+\bullet}Fe^{IV}O$ S = 1/2 species, as opposed to the reactions of nonheme $Fe^{IV}O$ species in solution, which transpire through the non-RM?

The most obvious difference that sets $Por^{+\bullet}Fe^{IV}O$ apart from the nonheme systems is that $Por^{+\bullet}Fe^{IV}O$ has a ligand radical accommodated in a_{2u} that acts as an electron sink, changing the way the electron is accepted from the substrate upon C-H activation. The situation in the nonheme case is therefore more akin to the S = 1 $PorFe^{IV}O$ Cpd II case, where a_{2u} is initially not used (see section 3.2 and Fig. 5). Hence, it is possible that this additional electronic repulsion (compared to Cpd I) is more disadvantageous to the rebound reaction in the nonheme case.

Another possible consequence of the a_{2u} orbital presence relates to the interaction geometry.[35] In Por$^{+\bullet}$Fe^{IV}O, the first electron is transferred to the π^*_{xz} orbital, and an internal electron transfer from the π^*_{xz} to a_{2u} orbital occurs. In the case of the low spin state, the rebound step then forms a C-O bond using the π^*_{yz} orbital (Fig. 8a), making it unnecessary for the substrate to relocate large distances, and the reaction is efficient.

For the nonheme cases, for most spin states, the substrate interacts with a different Fe^{IV}O orbital in the initial C-H activation step compared to the rebound step. This necessitates a relocation of the substrate radical intermediate in the second step, which possibly contributes to the barrier. Incidentally, this relocation occurs for the S = 3/2 and 5/2 states of PorFe^{IV}OH as well (Fig. 5), which both have small rebound barriers.

As the rebound barriers are generally low, these contributions to the barrier do not need to be large, and other yet to be identified factors may contribute to the barrier on such a small scale as well.

6. Conclusions

In contrast to the RM, the alternative dissociation pathway has received less attention over the years. Yet, it is hardly a surprising fact that once the substrate radical is formed, the dissociation energy should be minimal unless other factors, such as hydrogen bonds or constrained movements in enzymes, prevent the dissociation. The key to gain insight into the selectivity of RM vs. non-RM is therefore to understand the second step barrier. Only a rebound reaction with an extremely low or no energy barrier should be competitive; one example of this case is the S = 1/2 Por$^{+\bullet}$Fe^{IV}O species (see Table 1). We have described two factors that may influence the second step barrier for the different spin states of the Cpd I species (high-energy orbital interactions and electronic repulsion, see section 3.2). Reorganisation was also considered above when comparing heme vs. nonheme Fe^{IV}O species (section 5). Some substrate-dependant factors are expected to affect the second step barrier as well, such as the dissociation entropy and C-H bond strengths (section 4.2). The fact that hydroxylated products were found in the reaction does not unequivocally prove that a rebound reaction has occurred; other factors such as the total product yield, the oxidation state of inorganic product, and the effects of radical scavenger reactions (e.g., CCl_3Br and O_2) should also be taken into account. From a theoretical perspective, calculations on the non-rate limiting second step of the reaction should not be omitted if the rebound reaction is to be proved. In this respect, the participation of a second molecule of metal-oxo species to trap the radical during non-RM (Fig. 10) may reflect the higher capability of metal-oxo compared with metal-hydroxo to trap radicals. This feature of non-RM is left for future investigations.

Finally, given that the dissociation energy in many cases can be close to the rebound or desaturation barriers (Table 1), these studies do not necessarily exclude the existence of certain nonheme metal/ligand/substrate/solvent combinations that would prefer 1:1 rebound/desaturation reactions. Rather, the take-home message of this tutorial review is that caution is advised against assuming the involvement of a RM reaction without engaging in close investigations into the issue.

Table 1. Lowest second barrier height (ΔE_R) vs. dissociation energy (ΔE_D), collected from the literature, in kcal mol^{-1}.[a]

	Substrate	ΔE_R[b]	ΔE_D
Por$^{+\bullet}$Fe^{IV}O (S = 1/2) [c]	Methane	None[d]	2.7
Por$^{+\bullet}$Fe^{IV}O (S = 3/2) [c]	Methane	3.3	2.6
[Mn^{IV}O(Bn-TPEN)]$^{2+}$ [e]	Cyclohexane	12.8	1.6
[Fe^{IV}O(Bn-TPEN)]$^{2+}$ [f]	Cyclohexane	3.8	2.4
[Fe^{IV}O(Bn-TPEN)]$^{2+}$ [g]	Cyclohexane	1.9[h]	-13.0[h]
[Cr^{IV}O(TMC)Cl]$^{+}$ [i]	1,4-Cyclohexadiene	9.1	0.03
[Fe^{V}O(TAML)]$^{-}$ [j]	Cyclohexane	4.7	1.6
[Ru^{IV}O(terpy)(bpm)]$^{2+}$ [k]	Ethylbenzene	26.3[h]	-1.3[h]

[a] Energies refer to electronic energies unless otherwise noted. [b] Energies refer to either the rebound or desaturation barriers, whichever is lowest. [c] Data from ref. [22]. [d] A small reorganization barrier was found, which was smaller than the dissociation energy. [e] Data from ref. [34]. [f] Data from ref. [35]. [g] Data from ref. [25]. [h] Free energies (ΔG). [i] Data from ref. [36]. [j] Data from ref. [37]. [k] Data from ref. [38].

Acknowledgements

W.N. and K.-B.C. acknowledge the NRF of Korea through CRI (NRF-2012R1A3A2048842 to W.N.), GRL (NRF-2010-00353 to W.N.) and MSIP (2013R1A1A2062737 to K.-B.C.). S.S. acknowledges the Israel Science Foundation (ISF grant 1183/12). H.H. is grateful for a Nanyang Assistant Professorship.

References

1 P. R. Ortiz de Montellano and J. J. De Voss, *Nat. Prod. Rep.*, 2002, **19**, 477–493, and references therein.
2 S. Shaik, S. Cohen, Y. Wang, H. Chen, D. Kumar and W. Thiel, *Chem. Rev.*, 2010, **110**, 949–1017.
3 J. T. Groves, *J. Chem. Educ.*, 1985, **62**, 928–934.
4 J. T. Groves, G. A. McClusky, R. E. White and M. J. Coon, *Biochem. Biophys. Res. Commun.*, 1978, **81**, 154–160.
5 M. Sono, M. P. Roach, E. D. Coulter and J. H. Dawson, *Chem. Rev.*, 1996, **96**, 2841–2888, and references therein.
6 M. Newcomb and P. H. Toy, *Acc. Chem. Res.*, 2000, **33**, 449–455.
7 W. Nam, *Acc. Chem. Res.*, 2007, **40**, 522–531.
8 G. A. Hamilton, *J. Am. Chem. Soc.*, 1964, **86**, 3391–3392.
9 J. T. Groves and G. A. McClusky, *J. Am. Chem. Soc.*, 1976, **98**, 859–861.
10 J. T. Groves and M. Van der Puy, *J. Am. Chem. Soc.*, 1974, **96**, 5274–5275.
11 J. T. Groves and T. E. Nemo, *J. Am. Chem. Soc.*, 1983, **105**, 6243–6248.
12 J. T. Groves, T. E. Nemo and R. S. Myers, *J. Am. Chem. Soc.*, 1979, **101**, 1032–1033.
13 J. H. Dawson and M. Sono, *Chem. Rev.*, 1987, **87**, 1255–1276.
14 H. Schwarz, *Int. J. Mass Spectrom.*, 2004, **237**, 75–105, and references therein.
15 S. Shaik, H. Hirao and D. Kumar, *Nat. Prod. Rep.*, 2007, **24**, 533–552.
16 M. J. Park, J. Lee, Y. Suh, J. Kim and W. Nam, *J. Am. Chem. Soc.*, 2006, **128**, 2630–2634.
17 J. Rittle and M. T. Green, *Science*, 2010, **330**, 933–937.
18 H. Schwarz, *Isr. J. Chem.*, 2014, **54**, 1413–1431, and references therein.

19 J.-U. Rohde, J.-H. In, M. H. Lim, W. W. Brennessel, M. R. Bukowski, A. Stubna, E. Münck, W. Nam and L. Que Jr., *Science*, 2003, **299**, 1037–1039.
20 C. Krebs, D. Galonić Fujimori, C. T. Walsh and J. M. Bollinger, *Acc. Chem. Res.*, 2007, **40**, 484–492, and references therein.
21 C. V Sastri, J. Lee, K. Oh, Y. J. Lee, J. Lee, T. A. Jackson, K. Ray, H. Hirao, W. Shin, J. A. Halfen, J. Kim, L. Que Jr., S. Shaik and W. Nam, *Proc. Natl. Acad. Sci.*, 2007, **104**, 19181–19186.
22 S. Shaik, S. Cohen, S. P. de Visser, P. K. Sharma, D. Kumar, S. Kozuch, F. Ogliaro and D. Danovich, *Eur. J. Inorg. Chem.*, 2004, **2004**, 207–226.
23 E. J. Klinker, In *High-valent iron compounds supported by pentadentate ligands*, University of Minnesota, 2007.
24 A. Company, I. Prat, J. R. Frisch, D. R. Mas-Ballesté, M. Güell, G. Juhász, X. Ribas, D. E. Münck, J. M. Luis, L. Que Jr. and M. Costas, *Chem. – A Eur. J.*, 2011, **17**, 1622–1634.
25 D. Janardanan, D. Usharani, H. Chen and S. Shaik, *J. Phys. Chem. Lett.*, 2011, **2**, 2610–2617.
26 C.-M. Che, K.-W. Cheng, M. C. W. Chan, T.-C. Lau and C.-K. Mak, *J. Org. Chem.*, 2000, **65**, 7996–8000.
27 L. K. Stultz, M. H. V. Huynh, R. A. Binstead, M. Curry and T. J. Meyer, *J. Am. Chem. Soc.*, 2000, **122**, 5984–5996.
28 J. R. Bryant and J. M. Mayer, *J. Am. Chem. Soc.*, 2003, **125**, 10351–10361.
29 T. Kojima, K. Nakayama, K. Ikemura, T. Ogura and S. Fukuzumi, *J. Am. Chem. Soc.*, 2011, **133**, 11692–11700.
30 T. H. Parsell, R. K. Behan, M. T. Green, M. P. Hendrich and A. S. Borovik, *J. Am. Chem. Soc.*, 2006, **128**, 8728–8729.
31 J. F. Hull, D. Balcells, E. L. O. Sauer, C. Raynaud, G. W. Brudvig, R. H. Crabtree and O. Eisenstein, *J. Am. Chem. Soc.*, 2010, **132**, 7605–7616.
32 C. Arunkumar, Y.-M. Lee, J. Y. Lee, S. Fukuzumi and W. Nam, *Chem. – A Eur. J.*, 2009, **15**, 11482–11489, and references therein.
33 X. Wu, M. S. Seo, K. M. Davis, Y. M. Lee, J. Chen, K.-B. Cho, Y. N. Pushkar and W. Nam, *J. Am. Chem. Soc.*, 2011, **133**, 20088–20091.
34 K.-B. Cho, S. Shaik and W. Nam, *J. Phys. Chem. Lett.*, 2012, **3**, 2851–2856.
35 K.-B. Cho, X. Wu, Y. M. Lee, Y. H. Kwon, S. Shaik and W. Nam, *J. Am. Chem. Soc.*, 2012, **134**, 20222–20225.
36 K.-B. Cho, H. Kang, J. Woo, Y. J. Park, M. S. Seo, J. Cho and W. Nam, *Inorg. Chem.*, 2014, **53**, 645–652.
37 E. Kwon, K.-B. Cho, S. Hong and W. Nam, *Chem. Commun.*, 2014, **50**, 5572–5575.
38 S. N. Dhuri, K.-B. Cho, Y.-M. Lee, S. Y. Shin, J. H. Kim, D. Mandal, S. Shaik and W. Nam, *J. Am. Chem. Soc*, 2015, **137**, 8623–8632, and references therein.
39 S. Ye and F. Neese, *Proc. Natl. Acad. Sci.* , 2011, **108** , 1228–1233.
40 H. Hirao, D. Kumar, W. Thiel and S. Shaik, *J. Am. Chem. Soc.*, 2005, **127**, 13007–13018.
41 S. Shaik, H. Chen and D. Janardanan, *Nature Chem.*, 2011, **3**, 19–27.
42 F. Ogliaro, N. Harris, S. Cohen, M. Filatov, S. P. de Visser and S. Shaik, *J. Am. Chem. Soc.*, 2000, **122**, 8977–8989.
43 P. H. Toy, M. Newcomb and P. F. Hollenberg, *J. Am. Chem. Soc.*, 1998, **120**, 7719–7729.
44 J. Kaizer, E. J. Klinker, N. Y. Oh, J.-U. Rohde, W. J. Song, A. Stubna, J. Kim, E. Münck, W. Nam and L. Que Jr., *J. Am. Chem. Soc.*, 2003, **126**, 472–473.
45 H. Hirao, D. Kumar, L. Que Jr. and S. Shaik, *J. Am. Chem. Soc.*, 2006, **128**, 8590–8606.
46 R. P. Bell, *Proc. R. Soc. London, Ser. A Math. Phys. Sci.*, 1936, **154**, 414–429.
47 M. G. Evans and M. Polanyi, *Trans. Faraday Soc.*, 1938, **34**, 11–24.
48 J. Cho, J. Woo and W. Nam, *J. Am. Chem. Soc.*, 2012, **134**, 11112–11115.
49 F. T. de Oliveira, A. Chanda, D. Banerjee, X. Shan, S. Mondal, L. Que Jr., E. L. Bominaar, E. Münck and T. J. Collins, *Science*, 2007, **315**, 835–838.
50 M. Ghosh, K. K. Singh, C. Panda, A. Weitz, M. P. Hendrich, T. J. Collins, B. B. Dhar and S. Sen Gupta, *J. Am. Chem. Soc.*, 2014, **136**, 9524–9527.

Kyung-Bin Cho

Kyung-Bin Cho is now an emigrated immigrant to Sweden and obtained his M.Sc. in Physics at Stockholm University, Sweden. His Licentiate and Ph.D. degrees in Biophysics was earned at the same university under the guidance from Astrid Gräslund and Per Siegbahn regarding experimental and theoretical methods, respectively. After post-doc sessions in Canada (University of Windsor, James Gauld) and Israel (The Hebrew University of Jerusalem, Sason Shaik), he joined Wonwoo Nam's group as a Research Associate at Ewha Womans University in Seoul, Korea. Research interests now include application of theoretical methods, particularly DFT and DFT/MM, to the overlapping areas of biochemistry and inorganic chemistry in collaboration with experimentalists. Recent works include studies of metal-oxygen complexes and their reactivities.

Sason Shaik

Sason Shaik is a Saeree K. and Louis P. Fiedler Professor in Chemistry at The Hebrew University of Jerusalem, and director of The Lise Meitner-Minerva Center for Computational Quantum Chemistry. His research interests range from chemical bonding, to chemical reactivity, and all the way to metalloenzymes. His fascination with metalloenzymes and their synthetic models is rooted in their many spin- and electromeric states, which make their reactivity patterns intriguing and laden with surprises. Among his awards are the 2001 Kolthoff Award, the 2001 Israel Chemical Society Excellence Prize, the 2007 Schrödinger Medal of WATOC, and the 2012 August Wilhelm von Hofmann Medal of the German Chemical Society. He is a Fellow of the AAAS and WATOC, one of the "175 Faces in Chemistry" of the Royal Society of Chemistry, and a member of the International Academy of Quantum Molecular Science (IAQMS).

Hajime Hirao

Hajime Hirao was born in a quiet village of Hyogo, Japan. He received his BS and MS degrees from Kyoto University and his PhD from The University of Tokyo. He did his postdoc at The Hebrew University of Jerusalem, Emory University, and Kyoto University. He is currently assistant professor at Nanyang Technological University, Singapore. Since his undergraduate days, he has been interested in computational and theoretical aspects of chemistry, especially chemical reactions. Before starting his postdoc training, he also worked for three years on computer-assisted drug design in industry (Novartis in Japan). These have made his research interest lie primarily in the application of computational chemistry to chemical reactions in bioinorganic chemistry, homogeneous/heterogeneous catalysis, and medicinal chemistry.

Wonwoo Nam

Wonwoo Nam was born in Seoul, Korea. He received his B.S. (Honors) degree in Chemistry from California State University, Los Angeles and his Ph.D. degree in Inorganic Chemistry from University of California, Los Angeles in 1990. After one year postdoctoral experience at UCLA, he became an Assistant Professor at Hong Ik University in 1991. He moved to Ewha Womans University in 1994, where he is presently a Distinguished Professor of Ewha Womans University. His current research focuses on (1) the dioxygen activation and oxygen atom transfer by biomimetic models of heme and nonheme iron enzymes, (2) the synthesis, spectroscopic and structural characterization, and reactivity studies of nonheme metal-oxygen intermediates, (3) the elucidation of the mechanism of O-O bond formation in water oxidation reactions, and (4) the development of environmentally benign catalytic oxidation reaction

Key learning points

(1) While the rebound mechanism is well established for heme iron-oxo systems, it does not cover all the metal-oxo species.
(2) There is accumulating evidence that a radical dissociative, non-rebound mechanism is frequently occurring in oxidation reactions by nonheme metal-oxo species.
(3) Theoretical chemistry is a suitable tool for investigating the radical rebound step, which is usually not rate-limiting and therefore too fast to be probed by experimental means.
(4) Understanding the key orbital interactions gives you an insight into the chemistry occurring during the reaction.
(5) Do not assume a rebound mechanism just because there are hydroxylated products! A more detailed investigation is required.